Single-Column Models and Cloud Ensemble Models as Links between Observations and Climate Models

DAVID A. RANDALL AND KUAN-MAN XU

Department of Atmospheric Science, Colorado State University, Fort Collins, Colorado

RICHARD J. C. SOMERVILLE AND SAM IACOBELLIS

Scripps Institution of Oceanography, University of California, San Diego, La Jolla, California

(Manuscript received 4 January 1995, in final form 29 November 1995)

ABSTRACT

Among the methods that have been devised to test physical parameterizations used in general circulation models, one of the most promising involves the use of field data together with single-column models (SCMs) and/or cloud ensemble models. Here the authors briefly discuss the data requirements of such models and then give several examples of their use. Emphasis is on parameterizations of convection and cloud amount.

1. Introduction

How can we test parameterizations that have been developed or are under development for use in general circulation models (GCMs)? The first and most obvious approach is climate simulation itself. Here we "simply" perform a climate simulation and compare the results with observations, as illustrated in the top panel of Fig. 1. An advantage of this approach is that it tests the parameterization as it is intended to be used, that is, in climate simulation. There are several disadvantages, however. First, the results produced by a climate model are big and complicated and depend on all aspects of the model, so that it can be very difficult to attribute particular deficiencies of the results to particular aspects of the model's formulation. Second, climate simulations are computationally expensive and time consuming so that only a limited number of runs can be made. Finally, the individual weather systems simulated by climate models do not represent particular weather systems in particular places at particular times in the real world, so only statistical comparisons with observations are possible.

Figure 2 shows how a process-oriented field program can be used to validate and develop GCM parameterizations and also to validate remote sensing techniques. The GCM is represented by the "black box" at the top center. The GCM can be thought of as a collection of process models, including for example a model to predict cirrus cloud formation. When the GCM is run, it produces climate simulations. Satellite datasets like those produced by ERBE, ISCCP, and EOS can be used to evaluate the realism of the climate simulations.

The satellite datasets can tell us that a climate simulation has failed to reproduce some important aspect of the observed climate, such as the distribution of outgoing longwave radiation, but they cannot tell us *why* the model has failed. The cause of the failure must be determined in order to develop improvements to the model. The cause is a specific weakness or set of weaknesses in one or more of the process models that make up the GCM, for example, a problem with the cirrus cloud formation parameterization. To find the cause of the problem, it is therefore necessary to make measurements that relate directly to the process models themselves. One implication of this is that the process models must be formulated in such a way that they can be tested against data; this is not always the case, but it *should* always be the case.

A second approach is to use the parameterization in a forecast model, to do numerical weather prediction, and then compare the forecast with observations. This approach can also be represented by the top panel in Fig. 1. An important advantage of this approach is that it allows detailed comparison with data for individual weather events on particular days. It is expensive, however, since numerical weather prediction is an expensive business although, to the extent that the parameterization can be evaluated by using operational forecasts that must be done anyway, this problem can be dismissed. As with tests in climate models, the results produced by a numerical weather prediction model are big and complicated and depend on all aspects of the

Corresponding author address: Dr. David A. Randall, Department of Atmospheric Sciences, Colorado State University, Ft. Collins, CO 80523.

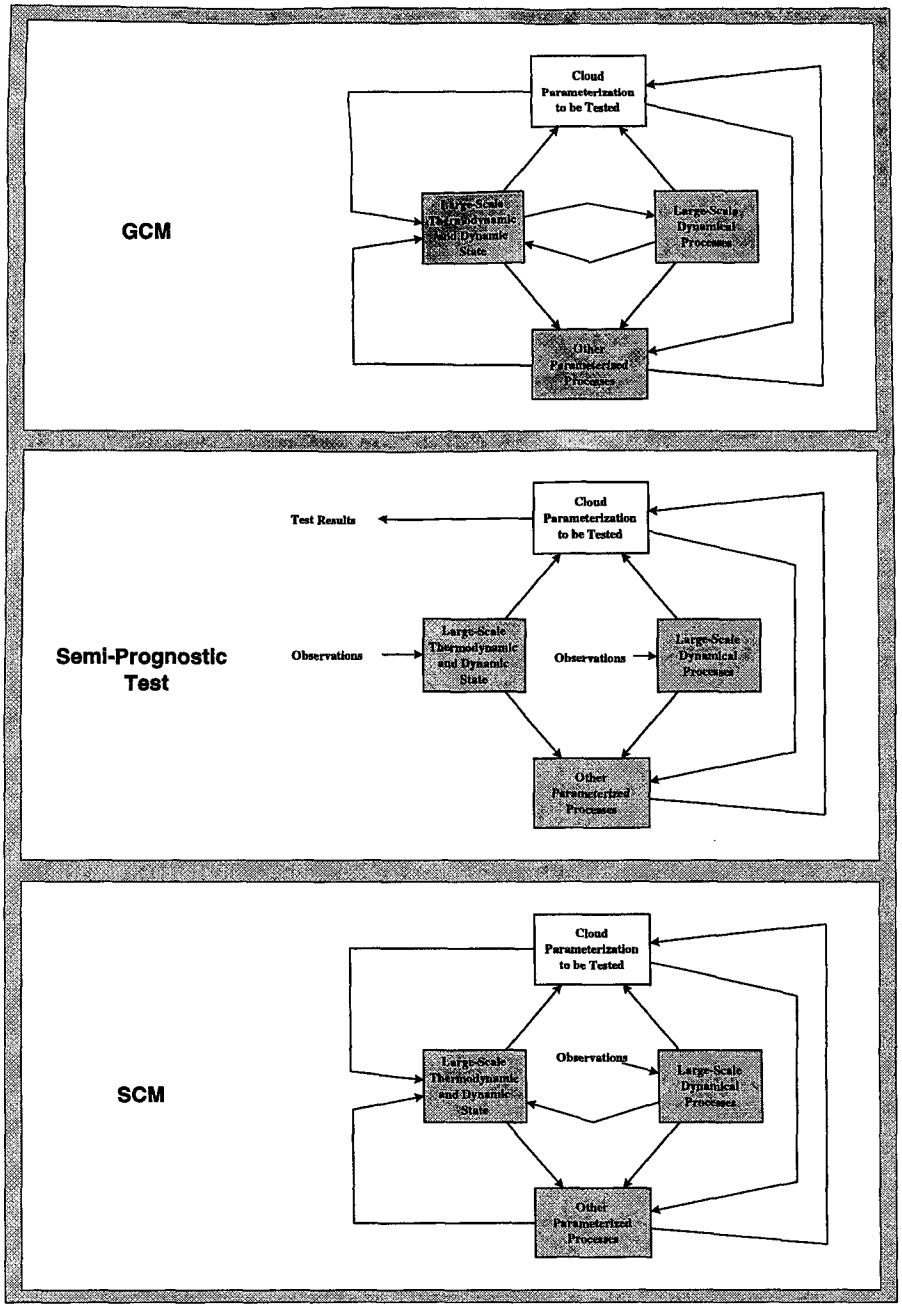

FIG. 1. Three ways to test parameterizations: Perform a climate simulation or weather forecast with the parameterization (top panel), perform a semiprognostic test (center panel), or run the parameterization in a single-column model (bottom panel). See text for details.

model, so that again it can be very difficult to attribute particular deficiencies of the forecasts to particular aspects of the model's formulation. A further difficulty is that a very elaborate data-ingest system is needed in order to do numerical weather prediction. Although such systems are in place at operational forecasting centers, they are not ordinarily available at climate modeling centers and would be prohibitively difficult to set up.

In brutally practical terms, the purpose of any parameterization is to compute certain "tendencies," that is, partial time rates of change due to the particular process represented by the parameterization. For example, one can say that the purpose of a radiation parameterization

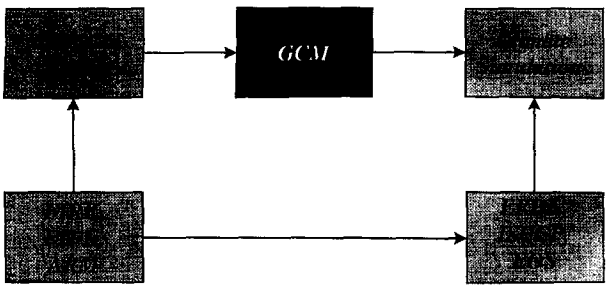

FIG. 2. Diagram illustrating the use of global data (ERBE, ISCCP, EOS) to evaluate the strengths and weaknesses of climate simulations and the use of field data on individual processes (from programs like FIRE, FIFE, and ARM) to evaluate the strengths and weaknesses of the process models that are used in GCMs. See text for further discussion.

is to compute radiative heating rates.[1] A parameterization can thus be tested by evaluating its ability to reproduce observed tendencies for a given large-scale situation. This can be done outside the climate model.

There are, in fact, two approaches that involve testing parameterizations outside the climate model, and predictably both have advantages and disadvantages. The first is the "semi-prognostic test," which was pioneered by Lord (1982) and has also been used by Kao and Ogura (1987) and Grell et al. (1991), among others. In this approach, which is illustrated in the center panel of Fig. 1, a parameterization or suite of parameterizations is exercised in the framework of a single atmospheric column, which can be thought of as a single column taken from a global climate model. A climate model can be considered to be a collection of many such columns, arranged to cover the entire earth and interacting with each other through a set of rules known as "large-scale dynamics." In a global climate model, neighboring grid columns provide information that is needed to determine what will happen within the grid column in question; for example, low-level convergence of mass from neighboring columns tends to produce rising motion, and horizontal advection produces tendencies of temperature and moisture. In the semiprognostic approach, there are no "neighboring grid columns," so all information that is needed and would otherwise be obtained from such columns is provided, instead, from observations. In some cases idealized data may be supplied in place of real observations.

Depending on the specific application, observations may also be used to determine the tendencies due to other processes that would be parameterized within a climate model. This is important because the algorithm for the computation of the tendencies produced by parameterization X on a given time step can require as input those produced by parameterization Y. As an example, if we were testing a cumulus parameterization, as Lord (1982) did, we might use observations to determine the radiative temperature tendencies and the effects of boundary-layer turbulence on the temperature and humidity of the air near the ground; both of these were in fact needed as input to the convective parameterization that Lord was testing.

To summarize, then, in a semiprognostic test observations are used to prescribe both the state of the atmospheric column and tendencies due to all processes except those associated with the parameterization to be tested. In addition, the current state of the atmosphere is also prescribed from observations. To the extent that the observations are error-free, any errors in the computed local time rates of change at a given time must be entirely due to problems with the parameterization being tested. The point is that this approach isolates the parameterization being tested from all other components of the model; the test is "clean." This is an important strength of the method. An additional strength is that the semiprognostic test is computationally very inexpensive compared to running a full large-scale model.

A semiprognostic test can be applied at a sequence of observation times, and we can think of these as being separated by "time steps." Because observations are used to specify the state of the atmosphere at each observation time, errors in the computed tendencies at the previous observation time have no effect; for convenience we summarize this by saying that there is "no feedback" from one time step to the next. This is both an advantage and a disadvantage. It is an advantage because it means that the time-averaged tendencies can be very wrong; a useful test, after all, is one that can be failed in many ways. For example, the parameterization might lead to a systematic erroneous warming tendency of 1 K per day at a certain level. After a sequence of many observation times, this would imply a huge time-accumulated temperature error at that level. The ability to produce such an error, or not, is a strength of the semiprognostic test. In other words, the semiprognostic test is a tough one because it is difficult to reproduce the observed time-mean tendencies.

The lack of feedback from one time step to the next is also a drawback, however, because parameterizations can have deficiencies that arise directly from such feedbacks; problems of this type cannot be detected with semiprognostic tests.

A further difficulty with semiprognostic tests is that the data requirements are very challenging. It is necessary to assemble a very complete picture of the large-scale circulation and the various physical processes not being tested in order to perform semiprognostic tests.

[1] Of course, a radiative transfer specialist would point out that an important additional motivation for the development of a radiation parameterization is to summarize some elements of our understanding of radiative transfer in a compact and relatively simple form. We certainly agree with this.

This is both expensive and complicated. Data requirements are discussed further below.

The second approach for testing climate model parameterizations outside of GCMs is somewhat similar to the semiprognostic test; it is called "single-column modeling" and is illustrated in the bottom panel of Fig. 1. Single-column modeling was pioneered, as a way of testing GCM parameterizations, by Betts and Miller (1986). As the name suggests, a single-column model (SCM) can be considered to be a grid column of a climate model, again considered in isolation from the rest of the model. As in the semiprognostic test, observations are used to specify what is going on in "neighboring columns," and observations may or may not also be used to specify tendencies due to some parameterized processes, other than those being tested. The key difference between single-column modeling and the semiprognostic test is that in an SCM the results obtained for one observation time are used to predict new values of the prognostic variables, which are then provided as input for the next observation time. Like semiprognostic tests, an SCM run can test a parameterization or a suite of parameterizations without complications from the rest of the global climate model, and it is very inexpensive, but it has demanding data requirements.

A problem with SCMs is that the time-averaged total tendencies have to be about right, that is, they have to be small since, for example, various feedbacks will act to prevent an erroneous 1 K per day warming for 30 consecutive days. A second problem is that although feedbacks that work inside a single column are active in an SCM, others, such as those involving the large-scale circulation, cannot be included. As a result, problems with the parameterization that involve such large-scale feedbacks cannot be detected using an SCM; they are best studied with a full climate model.

There is a second type of model that can be used to develop and test GCM parameterizations and can be driven with the same sort of observations as those needed to drive an SCM; this is a cloud ensemble model (CEM; sometimes called a "cumulus ensemble model" or "cloud-resolving model"). A CEM is a model with sufficient resolution to resolve (at least crudely) the structures of individual clouds (e.g., cumulus clouds), run over a spatial domain large enough to contain many clouds and for a time long enough to include many cloud life cycles. Most CEMs today are two-dimensional, although the increasing power of computers will allow this to change within a few years. The domain of a CEM can be considered to represent a single grid column of a GCM; in this way, a CEM is analogous to an SCM, but a CEM computes clouds and convection explicitly, whereas an SCM must parameterize them. CEMs are in use by many groups today (e.g., Yamazaki 1975; Krueger 1988; Nakajima and Matsuno 1988; Xu et al. 1992; Held et al. 1993; Krueger et al. 1995; Xu and Randall 1996a,b; Sui et al. 1994) in a variety of applications.

A CEM computes some things that are very difficult to observe, such as the vertical distribution of liquid water and ice. This simulated information is not a substitute for real observations because CEMs do contain parameterizations, notably microphysics and turbulence parameterizations, which introduce major uncertainties. CEM results are not reality. Nevertheless, CEM results can be judiciously compared with SCM results in order to diagnose problems with the latter.

It is possible to use either a CEM and an SCM to develop or test a parameterization, and it is advantageous to use both. An approach involving both is illustrated in Fig. 3. All information flows from the field data, which are used to drive the SCM and CEM and also to evaluate the simulations obtained. The results from the CEM can also be compared with those produced by the SCM. Finally, the parameterization tested in the SCM can be transferred directly to a three-dimensional GCM.

Parameterization tests with SCMs and CEMs can be of a "debugging" nature, or they can be physical tests like those indicated in Fig. 3. There are other possible applications, however. For example, an SCM or CEM can be forced with suitable output generated by a climate model or with idealized forcing designed to mimic a situation of interest, or we can use it to study radiative–convective equilibrium and similar idealized problems (e.g., Held et al. 1993; Sui et al. 1994; Rennó et al. 1994; Randall et al. 1994). In addition, an SCM and/or CEM can be used to untangle cause and effect relationships that are impossible to sort out directly from data or full GCM simulations; an example of this is presented later.

In section 2, we discuss the somewhat daunting data requirements of SCMs and CEMs when they are used to perform physical tests of parameterizations in a "case study" mode. Section 3 gives several examples

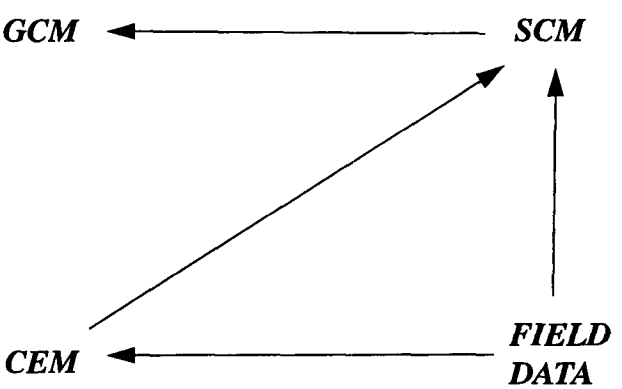

FIG. 3. Diagram illustrating how an SCM and a CEM can be used together to relate field data to a three-dimensional GCM. See text for details.

of the applications of SCMs and CEMs, including brief descriptions of some new results. Section 4 gives a summary and conclusions.

2. Data requirements

The data requirements for an SCM and a CEM are essentially the same. They are summarized in Table 1. The variables listed in the table are offered only as typical examples; certainly the particulars depend on the formulation of the model and the application at hand.

Among the data needed are time varying vertical profiles of the large-scale vertical motion and the tendencies of temperature and moisture due to horizontal advection. These are, of course, particularly troublesome quantities to observe and, in fact, they can only be obtained by very indirect means, which have been developed to overcome problems with missing data, instrument errors, and incomplete spatial and temporal coverage. Broadly speaking, there are two approaches; both are used in this paper. First, objective analysis methods can be used to combine measurements from various sources (e.g., rawinsonde data, wind profilers, etc.) in order to obtain synoptic descriptions of the large-scale dynamical and thermodynamic fields. These can then be differentiated (typically by approximate numerical methods) to infer wind divergence, horizontal gradients, etc. A particularly careful example of this approach is described by Ooyama (1987), who applied it to the GATE data.

A second approach is to make use of products obtained through data assimilation at operational numerical weather prediction centers (e.g., Bengtsson et al. 1982; Trenberth and Olsen 1988). Although such products are readily available and offer high-resolution global coverage with, potentially, high time resolution as well, the physical parameterizations of the forecast model do affect the results, particularly in data-sparse regions. This is a particularly worrisome problem for vertical motion and water vapor. For these reasons, it seems prudent to use pure objective analysis methods whenever possible. Assimilation products nevertheless offer unmatched spatial coverage and comprehensive information about the dynamical fields, and there is no question that they must play a very important role in driving SCMs and CEMs.

TABLE 1. Data requirements for SCMs and CEMs. These lists are intended to be illustrative rather than comprehensive.

Initial conditions
Temperature sounding
Water vapor mixing ratio sounding
Vertical distributions of cloud water and cloud ice
Horizontal wind components (vertical profile needed, but especially PBL values)
PBL depth (pressure units) and turbulence kinetic energy (not critical but useful)
Ground temperature and wetness
Mass of snow and/or liquid (e.g., dew or rain) stored on vegetation or ground surface
External parameters
Solar constant
Latitude, longitude, Julian day, and UTC
Surface characteristics (elevation, albedo, roughness, vegetation type, etc.)
Large-scale divergence
Tendencies of temperature and moisture due to horizontal advection
Pressure gradient force (if winds are predicted)
Momentum advection terms (if winds are predicted)
Data for model evaluation
All variables for which initial conditions are needed
Cloud amount as a function of height
Precipitation rate
Surface fluxes of sensible heat, moisture, and momentum
The same turbulent fluxes as functions of height
Solar and infrared (broadband) radiation fluxes, from the surface to the top of the atmosphere

3. Examples of the use of SCMs and CEMs

This section presents four examples in which SCMs and/or CEMs have been used. The first three examples involve testing parameterizations and the fourth involves separating cause and effect.

a. Tests of cloud amount parameterizations

Fractional cloudiness is a parameter that has been parameterized in large-scale models since the 1960s, and yet our physical understanding of what determines cloud amount has not advanced very far in the three decades that have passed since then. SCMs and CEMs now provide an opportunity to make more rapid progress toward the solution of this long-standing problem.

Xu and Krueger (1991) used the UCLA/U. Utah CEM to investigate the utility of several empirical cloud amount parameterizations based on different "predictors" or input variables. Among the predictors that they tested were the large-scale relative humidity, the large-scale vertical motion, the precipitation rate, and the convective mass flux. All of these predictors showed some utility, but none of them were skillful enough for quantitative applications.

Figure 4 shows an example of analysis performed in Xu and Krueger (1991). The total cloud amount and convective and stratiform cloud amounts are respectively correlated with the large-scale "predictors" such as relative humidity (Fig. 4a) and cloud mass flux (Fig. 4b). The coefficient of determination (R^2) is used to measure the utility of a diagnostic relation between "predictor" and "predictee." A value of R^2 higher than approximately 50% suggests a good relation. Figure 4 indicates that the total cloud amount cannot be adequately estimated at all levels with either predictor.

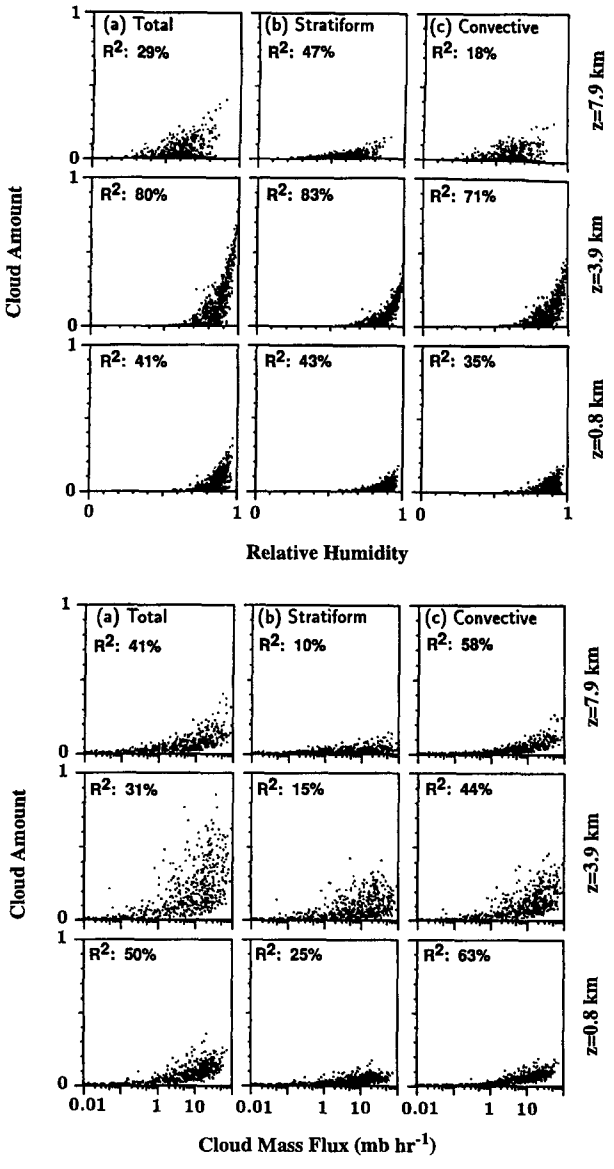

FIG. 4. (a) Scatterplots of total cloud amount versus relative humidity, stratiform cloud amount versus RH, and convective cloud amount versus RH at the 0.8-km, 3.9-km, and 7.9-km levels for data averaged over 128-km subdomains. (b) As in (a) except for using the cloud mass flux as the "predictor." There are 960 points in each scatterplot. The coefficient of determination (R^2) is also shown in the figure (from Xu and Krueger 1991).

Figure 4 also shows that the total cloud amount can be better estimated as the sum of separate estimates of stratiform and convective cloud amounts using different large-scale "predictors" than by an estimate of the total cloud amount using any single large-scale "predictor." The stratiform cloud amount can best be estimated by using relative humidity. The convective cloud amount can be diagnosed by using cloud mass flux. Xu and Krueger (1991) further showed that neither set of diagnostic relations depends significantly on the simulated cloud regime or horizontal averaging distance.

In a model that predicts the mass of condensed water (e.g., Sundqvist 1978; Tiedtke 1993; Fowler et al. 1995), *the condensate mixing ratio itself is an obvious candidate for use as a predictor of cloud amount.* A CEM is a very useful tool for the development of such an approach because a CEM can provide detailed information of the mixing ratio of cloud water and ice and that of fractional cloud amount, as well as other large-scale predictors. Figures 5 and 6 show CEM results based on ASTEX data (Albrecht et al. 1995) and GATE data (Reed et al. 1977). A more detailed discussion of these results will be presented elsewhere. ASTEX data were collected in a regime dominated by

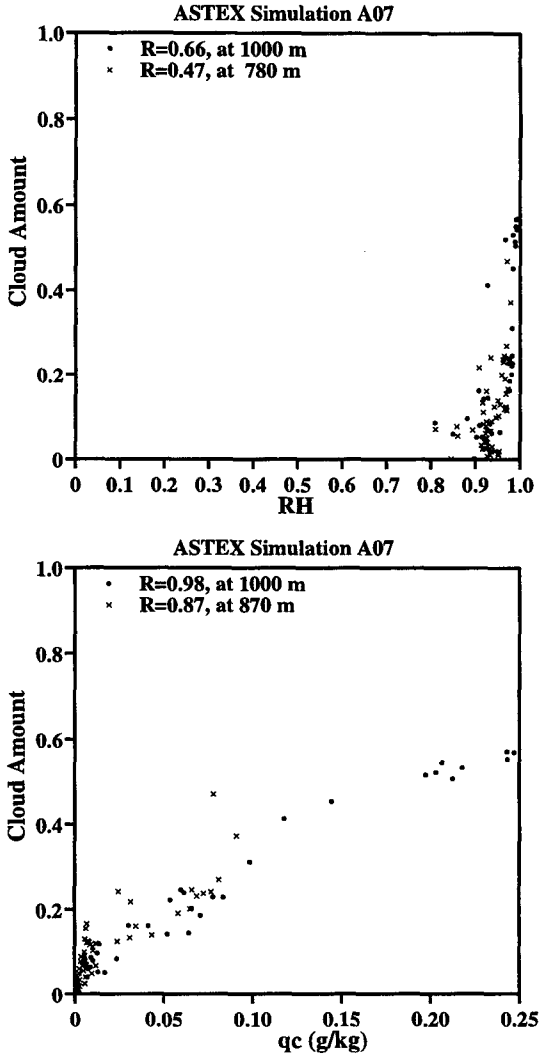

FIG. 5. Plots of cloud amount against relative humidity (top panel) and average cloud-water mixing ratio (bottom panel), as predicted by the CEM when driven by ASTEX data.

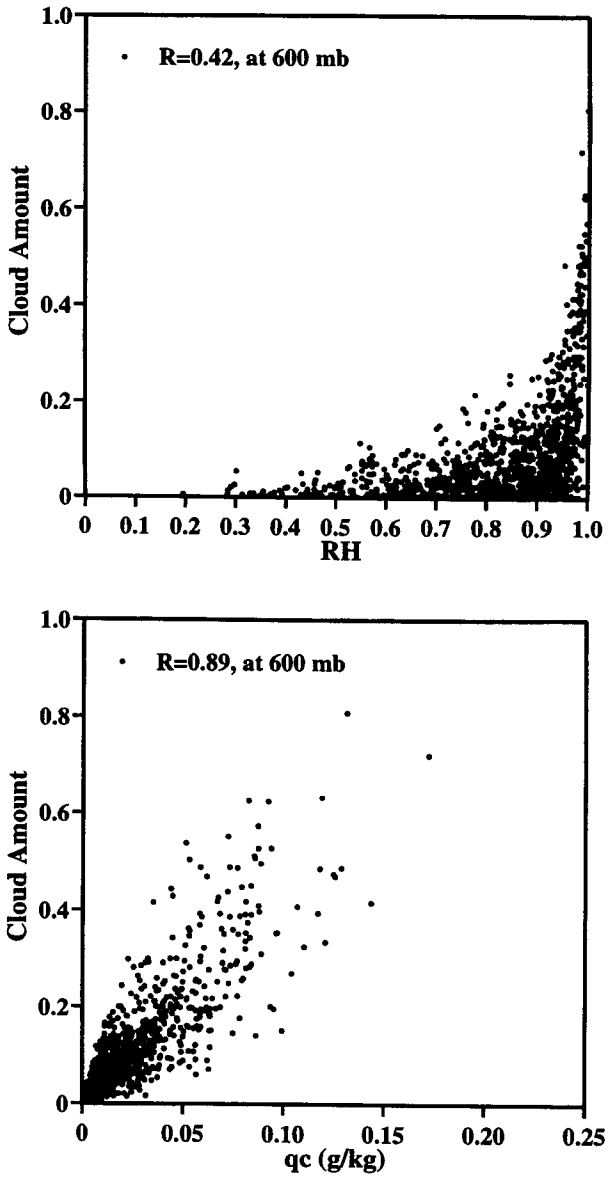

FIG. 6. Plots of cloud amount against relative humidity (top panel) and average cloud-water mixing ratio (bottom panel), as predicted by the CEM when driven by GATE data.

shallow cumuli with occasional thin stratiform clouds near the top of the convective layer, while GATE data were collected in a regime dominated by deep convection with extensive upper-tropospheric stratiform clouds. In Fig. 6, convective clouds are excluded by using a partitioning method based on draft intensity (Xu 1994). Both Fig. 5 and Fig. 6 show that the cloud amount is poorly predicted by the large-scale relative humidity (top panels) but is very well predicted by the domain-averaged cloud water mixing ratio (bottom panels) for these two distinctly different cloud regimes.

The lower panels of Figs. 5 and 6 show that the subgrid-scale cloud amount, f, is highly correlated with the large-scale average cloud water content, $\overline{q_c}$. Obviously, when $\overline{q_c} = 0$, $f = 0$, and as $\overline{q_c}$ increases f increases. It is also obvious that $f(q_c)$ must "curve over" as $\overline{q_c}$ continues to increase since f cannot exceed 1. What determines the initial slope of $f(q_c)$, that is, $(\partial f/\partial q_c)_{q_c=0}$? One fairly obvious consideration is that, when the large-scale relative humidity $\overline{\mathrm{RH}}$, is small, the cloud amount cannot increase all the way to 1, no matter how large $\overline{q_c}$ becomes. This suggests that $(\partial f/\partial q_c)_{q_c=0}$ should depend on $\overline{\mathrm{RH}}$, and in particular that $(\partial f/\partial q_c)_{q_c=0}$ should be relatively small when $\overline{\mathrm{RH}}$ is low. If $\overline{\mathrm{RH}}$ is close to 100%, then even a tiny amount of cloud water can be sufficient to produce a large cloud amount, at least in principle. These simple ideas suggest a parameterization of the form

$$f = (\overline{\mathrm{RH}})^p \left[1 - \exp\left(\frac{-\alpha q_c}{1 - \overline{\mathrm{RH}}} \right) \right]. \qquad (1)$$

Here the coefficient α and the exponent p can be determined empirically. Figure 7 gives a plot of f, as given by (1), as a function of $\overline{q_c}$ and $\overline{\mathrm{RH}}$, for $\alpha = 1000$ and $p = 1$. It is clear that Eq. (1) meets the requirements listed above. On the other hand, it has been written down on intuitive grounds with only weak, qualitative justifications. Much further work is needed to refine the parameterization and establish its practical utility for climate simulation.

b. *Sensitivity to parameters*

All parameterizations contain numerical parameters, and it is important to establish the sensitivity of model results to reasonable variations of these parameters. It is economically painful to perform large numbers of tests with large-scale models, but SCMs offer an op-

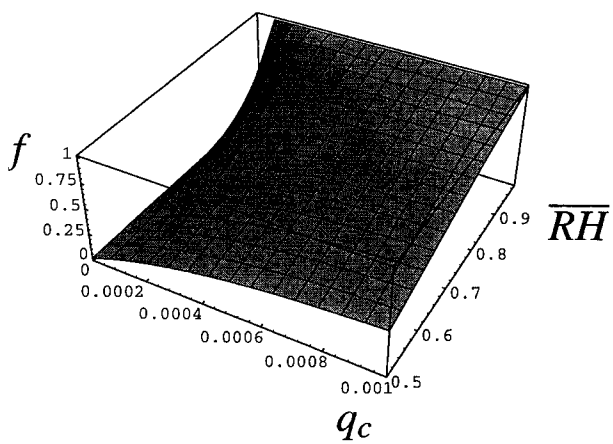

FIG. 7. Cloud amount, f, plotted as a function of the large-scale relative humidity, $\overline{\mathrm{RH}}$, and the grid-cell average cloud water mixing ratio, according to Eq. (1), using $\alpha = 1000$ and $p = 1$.

TABLE 2. The adjustable parameters studied in the sensitivity experiments. Given are a brief description of the parameter, the control value used, and the calculated sensitivities. As an example of how to interpret the sensitivity results, a 10% increase in $RH_{H,crit}$ results in a decrease in the average daily cloud amount of 0.062 (i.e., from 58.2% cloudy to 52% cloudy) and an increase in the net surface shortwave of 4.30 W m^{-2}.

Parameter	Description	Control value	f10%, CLD	f10%, NSW
	(a) Adjustable parameters of Sundqvist et al. (1989)			
c_0	Time scale for conversion of cloud droplets into raindrops (s^{-1})	1.0×10^{-4}	−0.014	+2.61
m_r	Threshold value for cloud water (kg kg^{-1})	3.0×10^{-4}	+0.014	−1.45
C_2	Parameter used to simulate enhanced release of precipitation in mixed-phase clouds (Bergeron–Findeisen mechanism) ($K^{-1/2}$)	0.5	−0.008	+1.06
T	Characteristic time scale for convection (s)	3600	+0.002	−0.27
U_{00}	Threshold relative humidity used to determine cloud amount	0.75	−0.036	+4.09
	(b) Adjustable parameters of Smith (1990)			
C_T	Characteristic time for conversion of cloud droplets into raindrops (s^{-1})	1.0×10^{-4}	−0.007	+2.37
C_W	Threshold value for cloud water (kg kg^{-1})	8.0×10^{-4}	−0.001	+0.34
C_A	Factor for increased conversion of cloud droplets to rain due to precipitation falling into layer from above (m^2 kg^{-1})	1.0	+0.003	−1.01
V_F	Fallout speed for frozen precipitation (m s^{-1})	1.0	−0.011	+2.61
C_{EV}	Time constant for evaporation or sublimation of precipitation (s^{-1})	2.0×10^{-4}	0.0	−0.40
RH_C	Threshold value of relative humidity at which point cloud formation begins	0.85	0.0	+1.76
	(c) Adjustable parameters of Slingo (1987)			
b	Used to relate convective cloud cover to convective precipitation amount	0.245	+0.006	−0.94
C_{crit}	Critical convective cloud cover for formation of cirrus anvils	0.3	−0.007	+0.62
$RH_{H,crit}$	Critical relative humidity for formation of extratropical and frontal high clouds (cirrus)	0.8	−0.062	+4.30
$RH_{M,crit}$	Critical relative humidity for formation of mid-level clouds	0.8	−0.035	+3.72
$RH_{L,crit}$	Critical relative humidity for formation of low-level clouds	0.8	−0.006	+2.04

portunity to fully explore the range of possibilities quickly and with minimal computational expense.

The SCM developed by Iacobellis and Somerville (1991a,b) has been used to test the sensitivity of radiatively important simulated quantities such as cloud amount and net surface shortwave radiation to choices in adjustable parameters in cloud liquid water parameterizations. The SCM incorporates a treatment of cloud optical properties, adopted by the second-generation GCM of the Canadian Climate Centre (McFarlane et al. 1992), in which optical properties are based on cloud liquid water contents (cf. Stephens 1978). The cloud liquid water prediction algorithms are adaptations of those of Sundqvist et al. (1989) and Smith (1990). Alternatively, the model can incorporate the cloud prediction parameterization of Slingo (1987), which does not include cloud liquid water as a prognostic variable. In this case, cloud optical properties are parameterized on temperature and pressure following Betts and Harshvardhan (1987), Platt and Harshvardhan (1988), and Somerville and Remer (1984). The model integrations in this study used the solar radiation parameterization of Fouquart and Bonnel (1980) and the longwave parameterization of Morcrette (1990).

The ECMWF Operational Analysis (2.5° × 2.5° with 16 levels) has been used to supply the horizontal convergences of heat, moisture, and momentum needed by the SCM at a location that corresponds to the southern Great Plains (SGP) site of the Atmospheric Radiation Measurement (ARM) Program. We have selected 16 test cases within the period from 1 January 1992 to 30 June 1993. These cases vary in duration from 5 to 13 days and were selected based (loosely) on the criteria of an increase and subsequent decrease in the observed relative humidity on time scales of about 3–6 days.

The SCM was run for each of the 16 test cases using control values of the adjustable parameters. The model was then rerun for each of the 16 test cases altering only one of the adjustable parameters. Thus, $16 \times N_p$ sensitivity runs were produced, where N_p is the number of adjustable parameters. For each adjustable parameter, we calculate a sensitivity parameter $f_{10\%,X}$ averaged over the 16 test cases, where $f_{10\%,X}$ is the expected change in quantity X for a 10% change in the adjustable parameter. This procedure is repeated for each of the three cloud parameterizations. Results are discussed below for daily averaged cloud amount (X = CLD) and daily averaged net surface shortwave radiation (X = NSW).

The results of the sensitivity experiments together with a brief description of each of the adjustable parameters are shown in Table 2. These results indicate that, of the parameters tested, the average daily cloud

amount and the net surface shortwave are most sensitive to changes in the parameters U_{00} and c_0 from Sundqvist's parameterization, C_T and V_F from Smith's parameterization, and $RH_{H,crit}$, $RH_{M,crit}$, and $RH_{L,crit}$ from Slingo's parameterization.

The parameters c_0 (Sundqvist) and C_T (Smith) both represent the timescale on which cloud droplets are converted to precipitation (m_r and C_W are also closely related). However, there are differences in the two cloud liquid water parameterizations that make direct comparisons difficult. For instance, the Sundqvist parameterization uses c_0 for both liquid and frozen precipitation, while the Smith parameterization uses C_T only for liquid precipitation and employs a separate relation for the formation of frozen precipitation.

The SCM results indicate that there is no sensitivity of the average daily cloud amount to changes in RH_C (Smith scheme), while there appears to be significant sensitivity of the NSW to changes in RH_C. At first this may appear to be a contradiction. However, further analysis indicates that changes in RH_C, while not having an effect on the average daily cloud amount (cloud cover), do affect the vertical distribution and/or total vertical cloud thickness, and these in turn affect the net shortwave radiation at the surface.

These sensitivity studies are based on only 16 test cases with no separation of convective and nonconvective events, and the resulting sensitivities cannot be fully interpreted until the uncertainties in the adjustable parameters have been quantified. As a consequence, the results presented here are very preliminary. However, the techniques described here, which are illustrative of those that can be used with SCMs, can be utilized to gain an improved understanding of current model parameterizations and to provide guidance in the development of new parameterizations.

This example illustrates that SCMs can be driven with data produced through the analysis and assimilation systems that have been developed to support operational numerical weather prediction.

c. *Tests of deep convection parameterizations*

Xu and Arakawa (1992) investigated the sensitivity of the Arakawa–Schubert (1974) cumulus parameterization to the horizontal resolution of large-scale models and the performance of a modified AS parameterization with convective downdrafts (Cheng 1989) using the CEM simulated data in Xu et al. (1992). The details of the AS parameterization will not be described here except as directly needed. Xu and Arakawa (1992) performed two different semiprognostic tests following a procedure similar to that used by Lord (1982). One uses the standard AS parameterization with the cloud work function (CWF) quasi-equilibrium (hereafter, control) and the other prescribes the CWF and its time change, thus allowing for CWF nonequilibrium, based on the CEM-simulated time change of the CWF (hereafter, nonequilibrium test). The CWF is defined as the rate of generation of cumulus kinetic energy due to work done by the buoyancy force per unit cloud-base mass flux (Arakawa and Schubert 1974).

The semiprognostic tests were performed for input data (T, q_v profiles and their large-scale and turbulence tendencies) averaged over various subdomains of the CEM with the widths of 512, 256, 128, and 64 km, as well as over 1 h in time. These tests correspond to applications of the parameterization in large-scale models with different horizontal resolutions. Mesoscale processes are partly resolved at the higher resolutions (e.g., 64 km). Figure 8 shows an example of test results obtained by Xu and Arakawa (1992). The figure shows the lag correlation between the apparent heat sources of simulation and parameterization for the 512, 256, 128, and 64 km subdomains. The time lag from −5 h to +5 h is chosen. A positive lag time indicates that the parameterized variable precedes the simulated one.

Figure 8 indicates that (i) the standard AS parameterization (i.e., the control test) performs reasonably well for all averaging distances and (ii) the impact of the CWF quasi-equilibrium assumption is not insignificant for the large subdomains. These suggest that the assumption is slightly worse when mesoscale processes are not even partially resolved. The explanation for this result is as follows. The large-scale forcing as defined by Arakawa and Schubert (1974; see also Lord 1982), which is mainly due to advective processes, is likely to become more dominant for smaller scales. On the other hand, the CWF, which is completely determined by the profiles of T and q_v, is not significantly scale-dependent. Therefore, the ratio of the time-change rate of CWF to the large-scale forcing decreases as the averaging distance decreases (Xu and Arakawa 1992).

On the other hand, Fig. 8 shows that the maximum correlation coefficients tend to decrease as the subdomain size decreases. Apparently the assumption of CWF quasi-equilibrium is not responsible for this decrease. It is possible that the inherently nondeterministic nature of the parameterization problem becomes relevant for small subdomains because smaller-scale phenomena become resolvable. In other words, we expect that nondeterministic errors are the largest for the smallest resolvable scale, while those for a larger-scale are not sensitive to the grid size used.

Another unique feature of the CEM results is that cumulus mass fluxes can be investigated; these are not directly available from observations. Figure 9a shows the updraft mass fluxes from the CEM, the fluxes as parameterized by the AS parameterization with updrafts only, and the fluxes as parameterized by a modified AS parameterization (Cheng 1989, hereafter ASC) with convective downdrafts. Figure 9b shows the downdraft mass fluxes from the CEM and the fluxes as parameterized by the modified AS parameterization. The nonequilibrium tests were performed for the results

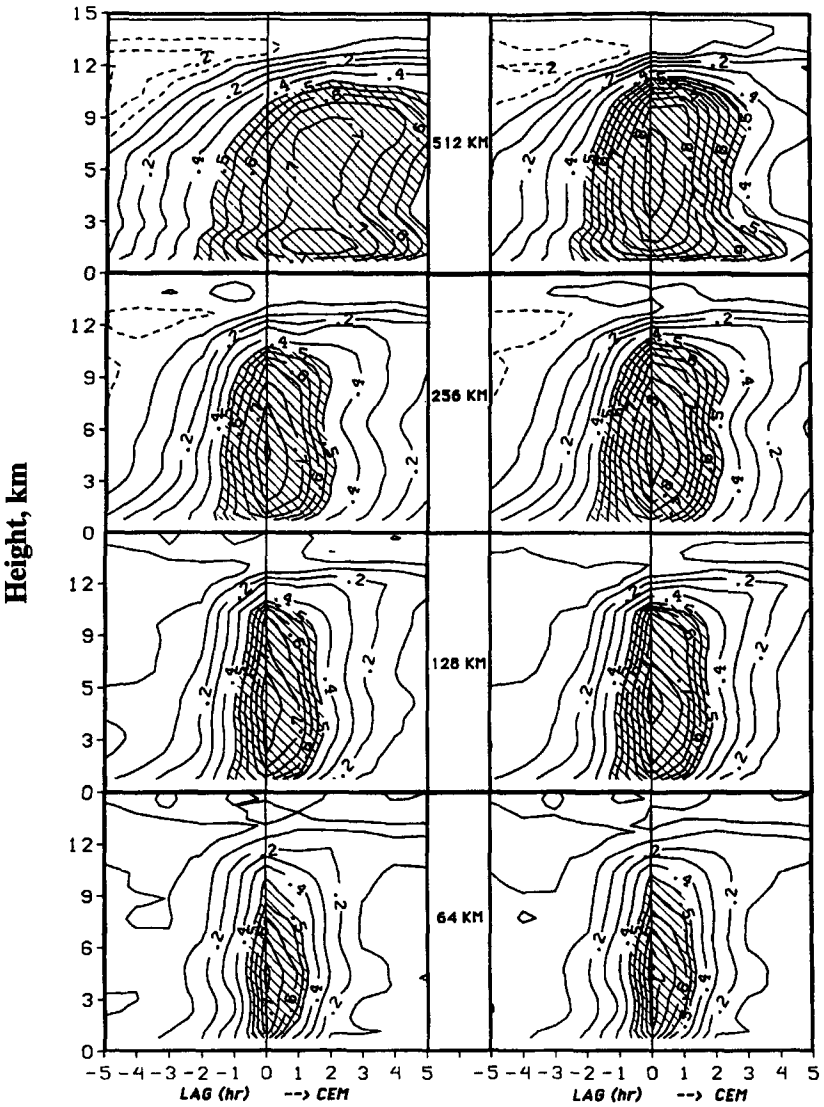

FIG. 8. Lag correlation coefficient between the apparent heat sources of simulation and parameterization as a function of height for the 512, 256, 128, and 64 km subdomains from the control run (left column) and the nonequilibrium test (right column). Hatched areas correspond to correlation coefficients greater than 0.5 with a contour interval of 0.05. The contour interval is 0.1 outside the hatched areas (from Xu and Arakawa 1992).

shown in Fig. 9. The comparison between simulated and parameterized mass fluxes gives the validity of the statistically steady cloud model and the mass-flux-based approach in cumulus parameterization because these parameterized results are free from the CWF quasi-equilibrium hypothesis. Figure 9 indicates that the updraft and downdraft mass fluxes from the ASC parameterization agree reasonably well with the simulated ones. The updraft mass flux in the original AS is smaller than that from the simulation. However, the updraft mass flux in the original AS parameterization is really the net upward mass flux. Therefore, it is better compared with the sum of updraft and downdraft mass flux from the CEM. These results indicate that the statistically steady cloud models used in the AS parameterization are basically valid. See Xu and Arakawa (1992) for further discussion.

d. Using SCMs and CEMs to untangle cause and effect: An investigation of the diurnal cycle of precipitation over the oceans

Randall et al. (1991, hereafter R91) used an SCM to investigate cause and effect issues that arise in connection with three mechanisms that have been suggested for producing daily oscillations of precipitation over the oceans.

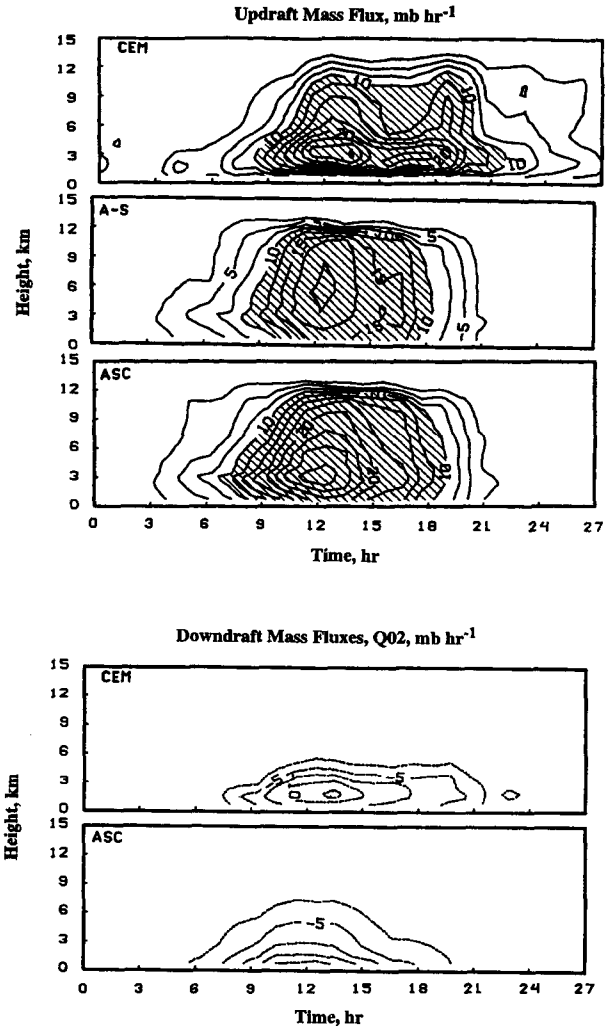

FIG. 9. The composited (a) updraft mass flux and (b) downdraft mass flux from the CEM simulation and from parameterizations of the original AS parameterization and a modified AS parameterization with convective downdrafts (ASC). The abscissa is the phase of the imposed large-scale advective processes. The contour intervals are 5 mb h^{-1} in (a) and 2.5 mb h^{-1} in (b); contours over 10 mb h^{-1} are hatched. (From Xu and Arakawa 1992.)

• *Direct radiation–convection interactions.* According to this simple hypothesis, atmospheric solar absorption during the day is concentrated in the upper portion of cloud masses associated with convection. This upper-level heating represents a stabilizing influence because it tends to decrease the lapse rate of temperature. At night, the destabilizing effects of longwave cooling dominate. This suggests that radiative forcing tends to favor more intense precipitation at night provided that there is some background process to force a time-mean precipitation. This hypothesis does not require diurnally varying large-scale motions, although it certainly does not preclude their existence and might account for them as a forced response to the combined effects of the radiative and latent heating.

• *Radiation–dynamics–convection interactions.* This is the hypothesis favored by Gray and Jacobsen (1977). Day–night differences in atmospheric radiative heating have one vertical profile in the cloudy, convectively active region and a different profile in neighboring clear regions. As a result, the cloudy region experiences cooling relative to its clear surroundings during the day and warming at night. These radiative effects induce day–night differences in vertical motions; in particular, upper-tropospheric rising motion is enhanced in the cloudy region during the night and suppressed in the cloudy region during the day. The result is an early morning precipitation maximum. There is observational evidence that the large-scale vertical motion does indeed undergo systematic day–night changes in convective weather systems over the tropical oceans. The mean upward vertical velocity in the disturbed marine atmosphere tends to be larger in the morning than in the evening. This somewhat complex mechanism involves both cloud–radiation interactions and spatially varying cloudiness, as well as diurnally varying large-scale vertical motions.

• *Remote influence of the continents.* According to this hypothesis, day–night differences in atmospheric heating over the continents drive large-scale motion systems that extend over (or propagate to) the neighboring oceans. These motions exhibit systematic daily variations associated with the diurnally varying continental heating that forces them. In this way, daily oscillations of precipitation over the oceans are excited.

R91 showed that the CSU GCM produces somewhat realistic diurnal variations of precipitation over the oceans when run in a fully configured three-dimensional earth simulation. This indicated that the model was a suitable tool for investigating the mechanisms that give rise to the observed diurnal variations.

They then simplified the model by omitting the continents and showed that a diurnal variation of precipitation occurs even on an ocean-covered planet. This eliminated the third hypothesis listed above.

They found, however, that the simulated large-scale vertical motion also undergoes diurnal variations, which are clearly correlated with precipitation events. This raised a "chicken and egg" question: does the *diurnally varying large-scale vertical motion* produce the *diurnal cycle of precipitation,* or vice versa?

Two hypotheses were consistent with the GCM results. In the first, diurnally varying radiation drives a diurnal signal in the large-scale vertical motion, which then drives the observed variations of the precipitation. This hypothesis is summarized in the top panel of Fig. 10. A second possibility is that the diurnally varying radiation drives the precipitation (through a mechanism to be described below), which then drives the vertical motion. This second hypothesis is summarized in the

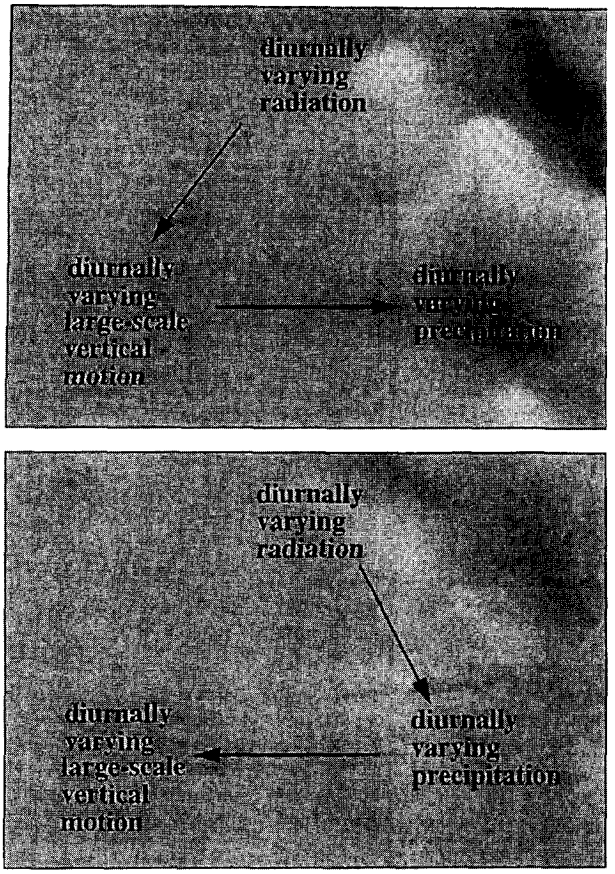

FIG. 10. Two alternative explanations for the observed relationships among the diurnal variations of radiation, precipitation, and large-scale vertical motion. See text for details.

lower panel of Fig. 10. Of course, it is also possible for some "mix" of these two mechanisms to occur.

It is very difficult if not impossible to distinguish between these two hypotheses on the basis of observations alone. Nature presents a diurnally varying radiation field, a diurnally varying large-scale vertical motion field, and a diurnally varying precipitation rate. We cannot perform experiments in nature to separate the interactions among these three signals. Similarly, a GCM cannot easily distinguish between the two hypotheses because such a model produces its own vertical motion field according to its governing equations. We cannot, for example, eliminate the diurnal signal in the large-scale vertical motion in the GCM to see if the diurnal variations of precipitation still occur.

The SCM (and/or a CEM) can be used to do exactly that. Because the large-scale vertical motion is and must be prescribed in an SCM, we can prescribe it in such a way that it has no systematic diurnal variation.

The SCM was driven with an idealized large-scale divergence field, based loosely on the observed composite GATE wave of Reed and his colleagues (Reed et al. 1977). The period of the wave was idealized to 97 hours (four days plus one hour). The model was initialized with a GATE sounding, and "spun up" for 100 simulated days. The model was then run for an additional 485 days (120 wave periods), sampling the results once per simulated hour, so that each wave phase was sampled exactly five times at each of the 24 hours of the day. This procedure was designed to prevent any systematic diurnal bias to enter through the prescribed time-varying vertical motion field.

As shown by R91, the SCM produces a systematic variation of precipitation over the period of the wave, with a maximum of about 25 mm day^{-1} when the upper-level wave divergence reaches a maximum, at the 11-km level, and a minimum of about 5 mm day^{-1} when the upper-level divergence has a minimum. These results are reasonable in light of the GATE data, as summarized by Reed et al. (1977).

In this way, the SCM was used to show that direct radiative–convective interactions can produce daily variability of the precipitation and other variables, with phase and amplitude similar to those observed over the tropical oceans, without any systematic diurnal variation of the vertical motion within the convective region. R91 concluded that the stabilization due to absorption of solar radiation, primarily by clouds, tends to suppress convection during the afternoon, relative to the period before sunrise, and that this mechanism alone can account qualitatively for the observed diurnal cycle of precipitation over the oceans.

This example illustrates that an SCM can produce realistic results when driven with observations and that experiments performed with the SCM can shed light on physical processes that would be difficult or impossible to isolate in a GCM (e.g., the SCM can isolate the role of large-scale vertical motion).

Recently, Xu and Randall (1995b) used a CEM to further explore these issues. The model that they employed is the two-dimensional UCLA/U. Utah CEM, developed at UCLA by S. Krueger and A. Arakawa. The CEM includes a third-moment turbulence closure, a three-phase microphysical parameterization, and the effects of the coriolis acceleration. Radiative heating has recently been incorporated in a version of the model being run at Colorado State University (Xu and Randall 1995a), following the methods of Harshvardhan et al. (1987), using the predicted distribution of cloud mass variables to determine the cloud optical properties. In typical applications, the horizontal domain is 512 km wide with a 2-km horizontal grid size. The depth of the CEM domain is typically 19 km, with a stretched coordinate and 33 layers. Near the surface the grid interval is 100 m, while near the model top it is 1000 m. The upper and lower boundaries are rigid. The lateral boundary conditions are cyclic. The initial thermodynamic conditions in a simulation are typically horizontally uniform. Clouds are initiated by introducing small, random temperature perturbations into the

lowest model layer for the first 30 minutes of integration.

Xu and Randall (1995b) performed two simulations, one with fully interactive radiative transfer and the other with horizontally uniform radiative heating rates determined from the domain-averaged heating rates of the fully interactive simulation. The diurnal variation of solar radiation and a time-invariant large-scale advective forcing are included in both simulations. The simulations were run for 15 days of physical time. A comparison of this pair of simulations can reveal whether or not the second hypothesis described above is important in the diurnal variation of oceanic precipitation. Figures 11a and 11b show the time sequence of the composited total and filtered surface precipitation rates, respectively, averaged in space over the entire CEM domain and over 1 hour in time. The filtered precipitation rate excludes all nondiurnal signals. In Fig. 11, I05 denotes the interactive simulation, and N05 the noninteractive one. Figure 11 indicates that the surface precipitation rate exhibits a diurnal variation in both simulations regardless of whether radiation is interactive or noninteractive. This suggests that the direct radiation–convection interaction is the dominant mechanism for the diurnal cycle. The difference between the two simulations is not totally negligible, however, in terms of the 2–3 h phase delay in the interactive simulation. The phase difference is related to the lagged response of the upper-tropospheric clouds to the radiative destabilization/stabilization in I05, as seen from the deviations of the outgoing longwave radiation (OLR) shown in Fig. 11c. The OLR in the cloudy regions (i.e., cloudy CEM columns) exhibits a larger phase delay with respect to the surface precipitation rate (solid line in Fig. 11b) than the OLR of the entire domain, which also includes cloud-free CEM columns. Figure 11c also shows that a smaller OLR does not necessarily correspond to a larger surface precipitation rate because a significant portion of the upper-tropospheric clouds do not produce precipitation at the ground (Xu 1994). Xu and Randall (1995b) performed further statistical analyses to quantify the importance of several cloud–radiation interaction mechanisms.

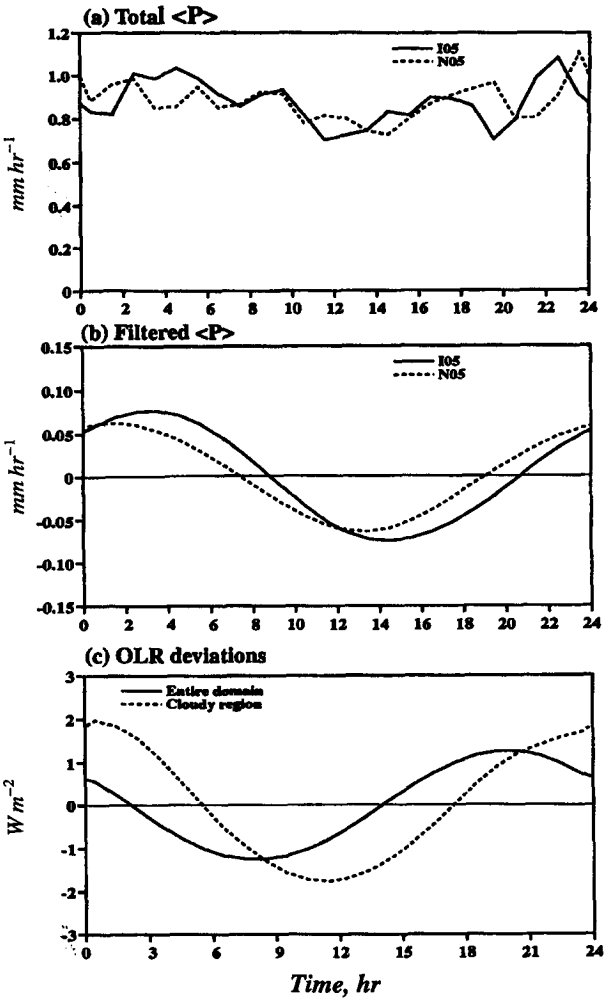

FIG. 11. Panels (a) and (b) show the time sequence of the composited total and filtered surface precipitation rates, respectively, which are averaged in space over the entire CEM domain and over 1 hour in time. I05 denotes the interactive simulation, and N05 the noninteractive one. Panel (c) shows the deviations of the outgoing longwave radiation (OLR).

4. Conclusions

Among the several methods for testing GCM parameterizations by comparison with observations, the single-column modeling approach has some unique advantages. SCM-based tests are inexpensive, and the results are not affected by errors arising from the other components of the model. Cloud ensemble models are a useful supplement to SCMs and can be used in much the same way with essentially the same data requirements.

The examples given here illustrate how SCMs and CEMs can be used to investigate basic physical questions, develop cloud amount parameterizations, and evaluate the sensitivity of model results to parameter changes. SCMs and CEMs will be particularly valuable for testing parameterizations of cloud formation, maintenance, and dissipation.

The data required to drive the SCMs and CEMs, and to evaluate their performance, is not easy to obtain. Field experiments such as ARM have the potential to provide uniquely valuable data for SCM-based parameterization testing. Efforts are under way to "package" data collected at ARM's Southern Great Plains Site in a form particularly convenient for use with SCMs and CEMs.

Acknowledgments. This study has been supported in part by the U.S. Department of Energy's ARM Program under Grant DE-FG02-92ER61363 to Colorado State

University. Computing resources were obtained from the National Energy Research Computer Center at the Lawrence Livermore National Laboratory. The research of Sam F. Iacobellis and Richard C. J. Somerville has been supported in part by the National Science Foundation (Grant ATM91-14109), the National Aeronautics and Space Administration (Grants NAG5-236 and NAG5-2238), the National Oceanic and Atmospheric Administration (Grant NA90AA-D-CP526), the U.S. Department of Energy under the Atmospheric Radiation Measurement (ARM) Program (Grant DE-FG03-90ER61061), Digital Equipment Corporation (Grant 1243), and the University of California Institutional Collaborative Research Program. Cindy Carrick assisted in the preparation of the manuscript.

REFERENCES

Albrecht, B. A., C. S. Bretherton, D. Johnson, W. H. Schubert, and A. S. Frisch, 1995: The Atlantic Stratocumulus Transition Experiment—ASTEX. *Bull. Amer. Meteor. Soc.*, **76,** 889–904.

Arakawa, A., and W. H. Schubert, 1974: The interaction of a cumulus cloud ensemble with the large-scale environment, Part I. *J. Atmos. Sci.*, **31,** 674–701.

Bengtsson, L., M. Kanamitsu, P. Kallberg, and S. Uppala, 1982: FGGE four-dimensional data assimilation at ECMWF. *Bull. Amer. Meteor. Soc.*, **63,** 29–43.

Betts, A. K., and M. J. Miller, 1986: A new convective adjustment scheme. Part II: Single column tests using GATE wave, BOMEX, ATEX, and arctic air-mass data sets. *Quart. J. Roy. Meteor. Soc.*, **112,** 693–709.

——, and Harshvardhan, 1987: Thermodynamic constraint on the cloud liquid water feedback in climate models. *J. Geophys. Res.*, **92,** 8483–8485.

Bretherton, C. S., E. Klinker, A. K. Betts, and J. A. Coakley Jr., 1995: Comparison of ceilometer, satellite and synoptic measurements of boundary layer cloudiness and the ECMWF diagnostic cloud parameterization scheme during ASTEX. *J. Atmos. Sci.*, **52,** 2736–2751.

Cheng, M.-D., 1989: Effects of downdrafts and mesoscale convective organization on the heat and moisture budgets of tropical cloud clusters. Part I: A diagnostic cumulus ensemble model. *J. Atmos. Sci.*, **46,** 1517–1538.

Fouquart, Y., and B. Bonnel, 1980: Computation of solar heating of the earth's atmosphere: a new parameterization. *Beitr. Phys. Atmos.*, **53,** 35–62.

Fowler, L. D., D. A. Randall, and S. A. Rutledge, 1996: Liquid and ice cloud microphysics in the CSU general circulation model. Part I: Model description and simulated microphysical processes. *J. Climate,* **9,** 489–529.

Gray, W. M., and R. W. Jacobsen, Jr., 1977: Diurnal variation of deep cumulus convection. *Mon. Wea. Rev.*, **105,** 1171–1188.

Grell, G. A., Y.-H. Kuo, and R. Pasch, 1991: Semiprognostic tests of cumulus parameterization schemes in the middle latitudes. *Mon. Wea. Rev.*, **119,** 5–31.

Harshvardhan, R. Davies, D. A. Randall, and T. G. Corsetti, 1987: A fast radiation parameterization for general circulation models. *J. Geophys. Res.*, **92,** 1009–1016.

Held, I. M., R. S. Hemler, and V. Ramaswamy, 1993: Radiative–convective equilibrium with explicit two-dimensional moist convection. *J. Atmos. Sci.*, **50,** 3909–3927.

Iacobellis, S. F., and R. C. J. Somerville, 1991a: Diagnostic modeling of the Indian monsoon onset. Part I: Model description and validation. *J. Atmos. Sci.*, **48,** 1948–1959.

——, and ——, 1991b: Diagnostic modeling of the Indian monsoon onset. Part II: Budget and sensitivity studies. *J. Atmos. Sci.*, **48,** 1960–1971.

Kao, C.-Y. J., and Y. Ogura, 1987: Response of cumulus clouds to large-scale forcing using the Arakawa–Schubert cumulus parameterization. *J. Atmos. Sci.*, **44,** 2437–2458.

Krueger, S. K., 1988: Numerical simulation of tropical cumulus clouds and their interaction with the subcloud layer. *J. Atmos. Sci.*, **45,** 2221–2250.

——, G. T. McLean, and W. Fu, 1995: Numerical simulation of the stratus-to-cumulations transition in the subtropical marine boundary layer. Part I: Boundary-layer circulation. *J. Atmos. Sci.*, **52,** 2851–2868.

Lord, S. J., 1982: Interaction of a cumulus cloud ensemble with the large-scale environment. Part III: Semi-prognostic test of the Arakawa–Schubert cumulus parameterization. *J. Atmos. Sci.*, **39,** 88–103.

McFarlane, N. A., G. J. Boer, J.-P. Blanchet, and M. Lazare, 1992: The Canadian Climate Centre second-generation general circulation model and its equilibrium climate. *J. Climate,* **5,** 1013–1044.

Morcrette, J.-J., 1990: Impact of changes to the radiation transfer parameterizations plus cloud optical properties in the ECMWF model. *Mon. Wea. Rev.*, **118,** 847–873.

Nakajima, K., and T. Matsuno, 1988: Numerical experiments concerning the origin of cloud clusters in the tropical atmosphere. *J. Meteor. Soc. Japan,* **66,** 309–329.

Ooyama, K., 1987: Scale-controlled objective analysis. *Mon. Wea. Rev.*, **115,** 2476–2506.

Platt, C. M. R., and Harshvardhan, 1988: Temperature dependence of cirrus extinction: Implications for climate feedback. *J. Geophys. Res.*, **93,** 11 051–11 058.

Randall, D. A., Harshvardhan, and D. A. Dazlich, 1991: Diurnal variability of the hydrologic cycle in a general circulation model. *J. Atmos. Sci.*, **48,** 40–62.

——, Q. Hu, K.-M. Xu, and S. K. Krueger, 1994: Radiative–convective disequilibrium. *Atmos. Res.*, **31,** 315–327.

Reed, R. J., D. C. Norquist, and E. Recker, 1977: The structure and properties of African wave disturbances as observed during Phase III of GATE. *Mon. Wea. Rev.*, **105,** 317–333.

Rennó, N. O., K. A. Emanuel, and P. H. Stone, 1994: Radiative–convective model with an explicit hydrologic cycle. Part I: Formulation and sensitivity to model parameters. *J. Geophys. Res.*, **99,** 14 429–14 442.

Slingo, J., 1987: The development and verification of a cloud prediction scheme for the ECMWF model. *Quart. J. Roy. Meteor. Soc.*, **113,** 899–927.

Smith, R. N. B., 1990: A scheme for predicting layer clouds and their water content in a general circulation model. *Quart. J. Roy. Meteor. Soc.*, **116,** 435–460.

Somerville, R. C. J., and L. A. Remer, 1984: Cloud optical thickness feedbacks in the CO_2 climate problem. *J. Geophys. Res.*, **89,** 9668–9672.

Stephens, G. L., 1978: Radiation profiles in extended water clouds. Part II: Parameterization schemes. *J. Atmos. Sci.*, **35,** 2123–2132.

Sui, C.-H., K.-M. Lau, W.-K. Tao, and J. Simpson, 1994: The tropical water cycle and energy budget in a cumulus ensemble model. Part I: Equilibrium climate. *J. Atmos. Sci.*, **51,** 711–728.

Sundqvist, H., 1978: A parameterization scheme for non-convective condensation including prediction of cloud water content. *Quart. J. Roy. Meteor. Soc.*, **104,** 677–690.

——, E. Berge, and J. E. Kristjansson, 1989: Condensation and cloud parameterization studies with a mesoscale numerical weather prediction model. *Mon. Wea. Rev.*, **117,** 1641–1657.

Tiedtke, M., 1993: Representation of clouds in large-scale models. *Mon. Wea. Rev.*, **121,** 3040–3061.

Trenberth, K. E., and J. G. Olson, 1988: An evaluation and intercomparison of global analyses from the National Meteorological Center and the European Centre for Medium-Range Weather Forecasts. *Bull. Amer. Meteor. Soc.*, **69,** 1047–1057.

Xu, K.-M., 1994: A statistical analysis of the dependency of closure assumptions in cumulus parameterization on the horizontal resolution. *J. Atmos. Sci.*, **51,** 3674–3691.

——, and S. K. Krueger, 1991: Evaluation of cloudiness parameterizations using a cumulus ensemble model. *Mon. Wea. Rev.*, **119,** 342–367.

——, and A. Arakawa, 1992: Semi-prognostic tests of the Arakawa–Schubert cumulus parameterization using simulated data. *J. Atmos. Sci.*, **49,** 2421–2436.

——, and D. A. Randall, 1995a: Impact of interactive radiative transfer on the macroscopic behavior of explicitly simulated cumulus ensembles. Part I: Radiation parameterization and sensitivity tests. *J. Atmos. Sci.*, **52,** 785–799.

——, and ——, 1995b: Impact of interactive radiative transfer on the macroscopic behavior of explicitly simulated cumulus ensembles. Part II: Mechanisms for cloud-radiation interactions. *J. Atmos. Sci.*, **52,** 800–817.

——, A. Arakawa, and S. K. Krueger, 1992: The macroscopic behavior of cloud ensembles simulated by a cloud ensemble model. *J. Atmos. Sci.*, **49,** 2402–2420.

Yamazaki, M., 1975: A numerical experiment of the interaction between cumulus convection and larger-scale motion. *Pap. Meteor. Geophys.*, **26,** 63–91.